Scientific Research Publishing

Open Journal of Civil Engineering, 2026, 16(3), 687-706
https://www.scirp.org/journal/ojce
ISSN Online: 2164-3172
ISSN Print: 2164-3164

Geotechnical and Thermo-Physical Characteristics of a Fine-Grained Lateritic Soil Excavated from a Road Construction Site: Experimental Study

Soumaïla Gandema[1], François Dabilgou[1], Marie Therese Marame Mbengue[2], Rimyalegdo Kiébré[3], Guillaume Zamantakonè Ki[1], Marcel Bawindsom Kébré[1], Adamah Messan[2]

[1]Laboratoire de Matériaux et Environnement (LAME), Université Joseph KI-ZERBO, Ouagadougou, Burkina Faso
[2]Laboratoire Eco-Matériaux et Habitats Durables (LEMHaD), Institut International d'Ingénierie de l'Eau et de l'Environnement (2iE), Ouagadougou, Burkina Faso
[3]Département de Physique, Université Lédea Bernard OUEDRAOGO, Ouahigouya, Burkina Faso
Email: soumaila_gandema@ujkz.bf

How to cite this paper: Gandema, S., Dabilgou, F., Mbengue, M.T.M., Kiébré, R., Ki, G.Z., Kébré, M.B. and Messan, A. (2026) Geotechnical and Thermo-Physical Characteristics of a Fine-Grained Lateritic Soil Excavated from a Road Construction Site: Experimental Study. *Open Journal of Civil Engineering*, **16**, 687-706.
https://doi.org/10.4236/ojce.2026.163034

Received: August 23, 2026
Accepted: September 20, 2026
Published: September 23, 2026

Abstract

The durability of road infrastructure in Sub-Saharan Africa represents a major challenge, exacerbated by growing climate hazards and the depletion of conventional materials. Road construction projects consume non-renewable natural resources such as lateritic gravels, as well as locally scarce resources such as water. In response to the need to preserve these resources, the valorization of local excavated materials—previously considered unsuitable for reuse—appears promising. This manuscript presents a comprehensive characterization of an excavated fine lateritic soil from a road construction site in Bassinko (Burkina Faso), with a view toward its reuse in earthworks. The objective is to evaluate its thermo-hydraulic and mechanical properties to provide a sustainable alternative to the exploitation of traditional lateritic borrow pits, which are becoming increasingly scarce. Experimental investigations on the material focused on determining its physical and morphological properties (particle density, Atterberg limits, methylene blue value, particle size distribution, Proctor characteristics), thermal conductivity (in dry and saturated states), the soil-water characteristic curve (SWCC), and mechanical bearing capacity (CBR/IPI). The results show that thermal conductivity is highly dependent on the degree of saturation, increasing from 0.458 W·m^{-1}·K^{-1} in the dry state to 1.826 W·m^{-1}·K^{-1} at saturation, illustrating the formation of aqueous thermal bridges. The analysis of the SWCC, modeled using the Van Genuchten equation, reveals high Van Genuchten modeling parameters P_{dry} and P_{sat} (1.85 MPa and 1.03

MPa, respectively), confirming a fine microporous structure. Although soaking causes a drop in the CBR index—decreasing from 50% to 20% for modified energy and from 25% to 17% for standard energy due to the dissipation of matric suction—the material maintains a stable S4 bearing class. Despite an initial classification often deemed "mediocre," this soil exhibits sufficient immediate bearing capacity and low swelling potential ($G < 1\%$). Its reuse will limit the opening of new borrow sites, thereby reducing the ecological footprint and costs of road infrastructure projects.

Keywords

Excavated Materials, Experimental Characterization, Sandy-Clay Soil, Road Earthworks, Sustainable Development

1. Introduction

Road projects require the mobilization of large quantities of soil. In tropical Africa, lateritic gravels remain the benchmark materials. Particularly in Burkina Faso, where the paved network is still very limited—with only 26.7% of the classified network being paved [1]—the demand for lateritic gravel is increasing due to numerous road projects currently underway or in the planning stages [1]-[3]. Given this situation, the management of natural resources constitutes one of the primary challenges in road development [4] [5]. Indeed, standard road construction practice involves supplying large volumes of lateritic gravel from borrow pits, which are becoming increasingly scarce and are often located far from construction sites [6]. In addition to the depletion of this resource, which is advantageous for use in base and sub-base layers [4], extraction and transport methods cause negative environmental impacts (such as gas emissions from machinery and high aerosol loading in surrounding areas) and social consequences, notably the loss of potentially arable land for local populations [7] [8].

To address one of the primary challenges—namely the overexploitation of lateritic gravels—the use of local materials located near construction sites proves to be a relevant solution. Indeed, in Burkina Faso specifically, and in tropical and Sahelian countries more generally, significant proportions of swelling or low-swelling sandy-clay soils are encountered at road construction sites [9]-[12]. However, when these soils are used in road embankments, they are subjected to mechanical stresses (road traffic) [13], thermal stresses (due to excessive solar radiation), and hydraulic stresses caused by capillary rise, climatic hazards (flooding, drought), or nearby human activities (excessive irrigation, water pipe leaks, etc.) [14] [15]. These stresses can lead to significant changes in soil properties, potentially compromising the stability and durability of the structures. Consequently, the reuse of these local soils in road embankments is only feasible when they are treated following an exhaustive characterization of their thermo-hydro-mechanical properties. Such treatment enables them to achieve sufficient performance levels to withstand the various mechanical and environmental stresses to which they will be subjected (road traffic, climate, etc.) [12] [16] [17].

A growing body of literature has explored the potential of these local materials in tropical Africa [10] [17]-[25]. As highlighted by Reiffsteck *et al.* [23], this approach significantly reduces construction costs, notably by limiting the transport of borrow materials and the disposal of excavated soil, while contributing to the sustainable management of natural resources. This practice also aligns with the current context of sustainable development and environmental protection [26].

Although numerous studies have established the potential of low-swelling fine-grained soils as earthwork materials, their behavior in tropical climates is not yet fully understood, as it is complex and depends on several factors. This uncertainty limits their reuse. Furthermore, current specifications for their use in road infrastructure are essentially based on simple identification parameters. In light of these findings, this manuscript proposes an in-depth experimental characterization of a fine-grained soil excavated from a road construction site. It successively addresses the physical and morphological properties of the material, its thermal and hydro-dynamic characteristics, and finally its identification for potential use in road infrastructure.

2. Location of the Road Construction Site

Within the framework of the development and paving of urban roads in the cities of Ouagadougou and Bobo-Dioulasso, the Burkinabe government has initiated the paving of the main access road to the Bassinko district (located on the map in **Figure 1**). This locality is situated on the northwestern outskirts of Ouagadougou (Burkina Faso). The soil sample used in the present study was collected from this road construction site: a 6.17 km section connecting the locality to National Road RN02. The sample was collected from one of four (4) disposal sites (shown in **Figure A1** in Appendix A). A quantity of approximately 500 kg of soil was sampled from the non-organic excavated layer at depths ranging from 0.3 m to over 1 m in some places.

3. Experimental Characterization of Physical and Morphological Properties

3.1. Physical Properties of the Soil

The physical characterization of the soil includes the determination of the specific gravity of solid grains, bulk density, *in-situ* void ratio, saturated water content, Atterberg limits, and optimal compaction parameters.

3.1.1. Particle Density and Specific Weight

The specific weight or unit weight (γ_s) of a soil is used in civil engineering to determine the weight of a structure designed to support specific loads while remaining intact and within its deformation limits. Its laboratory determination is based on the measurement of the particle density (or real density) ρ_s of the

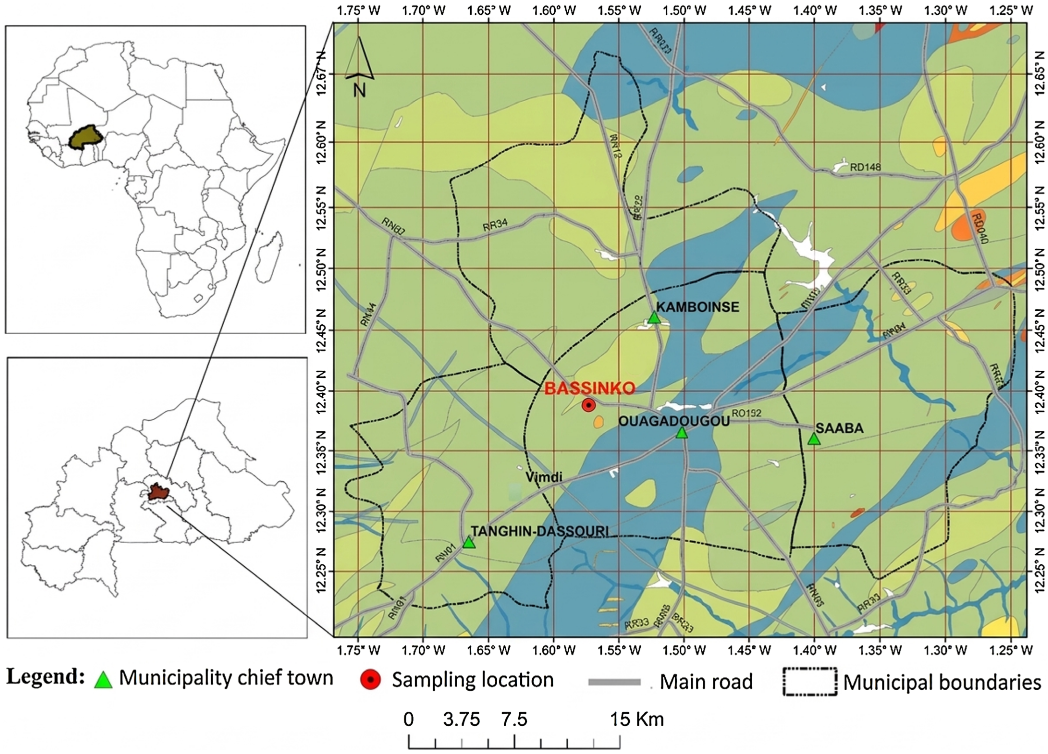

Figure 1. Location of the sampling site.

soil's solid grains (NF-EN-ISO-17892-3, 2015). The experimental setup and key laboratory procedure steps are illustrated in Appendix A (Figure A2).

The test was conducted on a single specimen. The values obtained for the particle density (ρ_s) and specific gravity (γ_s) are recorded in Table 1. The determined value of ρ_s is close to the standard particle density value typically used for soils when measurements are unavailable, namely 2650 kg·m^{-3}.

Table 1. Particle density and specific weight.

Particle density	Specific weight
$\rho_s\left[\text{kg}\cdot\text{m}^{-3}\right]$	$\gamma_s = \rho_s \times g\left[\text{kN}\cdot\text{m}^{-3}\right]$
2631	26.3

3.1.2. Atterberg Limits

Atterberg limits, or soil consistency limits, are used to identify and classify the soil. They also allow for the prediction of its behavior during earthwork phases and/or when subjected to mechanical stress (allowable stress, modulus of elasticity). Standard NF-EN-ISO-17892-12 (2018) specifies the methods for their determination, namely the liquid limit (w_L) and the plastic limit (w_P). These are determined on the fine fraction of the material passing through a 0.4 mm sieve. The plasticity index I_P of the soil corresponds to the difference between w_L and w_P. It indicates the extent of the plastic range and is commonly used to characterize soil clayiness. Table 2 summarizes these three soil parameters. Based on the obtained values, the studied soil, with an I_P between 12 and 22, is classified as moderately clayey [27].

Table 2. Atterberg limits of the soil.

Liquid limit	Plastic limit	Plasticity index
$w_L\,[\%]$	$w_P\,[\%]$	$I_P = w_L - w_P\,[\%]$
31.7	16.1	15.6

3.1.3. Methylene Blue Value of the Soil

The methylene blue value (MBV), which characterizes the clayiness of a soil, is determined according to standard NF-EN-933-9 (1999). The test data and the resulting VBS are recorded in **Table 3**. According to the GTR classification system [27], which uses the VBS for soil identification, the studied material is classified as a low-plasticity clayey sand.

Table 3. Methylene blue value of the soil.

Blue solution concentration	Solution volume	Soil mass	Blue value
$\rho_B\left[\mathrm{g\cdot dm^{-3}}\right]$	$V_B\left[\mathrm{cm^3}\right]$	$m_s\,[\mathrm{g}]$	$\mathrm{MBV} = \dfrac{\rho_B \times V_B}{m_s}$
10	90	60	1.5

3.1.4. Proctor Characteristics

The Proctor characteristics of the soil are presented below. **Figure 2** shows the Proctor curves obtained according to standard NF-P94-093 (2014). The 80% and 100% saturation curves (zero air voids curves) are also illustrated. **Table 4** summarizes the optimal compaction characteristics of the studied soil.

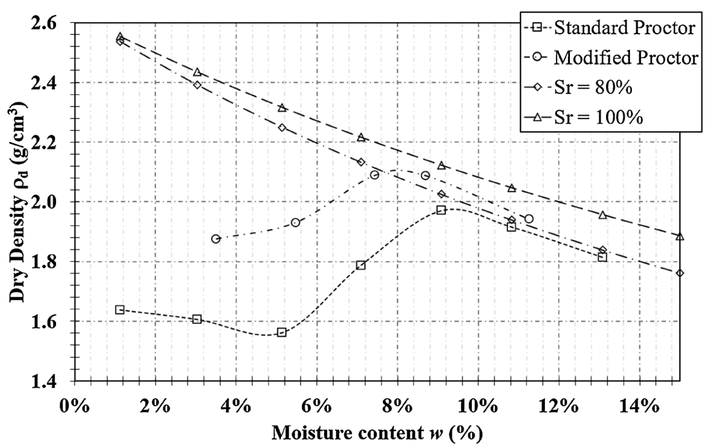

Figure 2. Proctor curves.

The curves, which are relatively flat, reveal a wide range of compaction water contents that allow the material to achieve optimal mechanical performance. The optimal characteristics of this soil (**Table 4**) are virtually identical to those reported by Savadogo *et al.* [24]. Furthermore, the Modified Proctor dry density (ρ_{OPM}) is in the same range as those measured by Mbengue *et al.* [21]. In contrast, the optimal water content (w_{OPM}) obtained for this soil is slightly lower, indicating a higher clay particle content in the studied soil.

Table 4. Proctor characteristics of the soil.

Standard proctor		Modified proctor	
$w_{OPN}\,[\%]$	$\rho_{OPN}\left[g\cdot cm^{-2}\right]$	$w_{OPM}\,[\%]$	$\rho_{OPM}\left[g\cdot cm^{-2}\right]$
9.4	1.98	8.0	2.10

3.2. Morphological Characterization—Particle Size Distribution

The particle size distribution (PSD) of the soil is determined according to standard NF-EN-ISO-17892-4 (2018). The described methodology employs both sieve analysis (for particles larger than 80 μm) and hydrometer analysis (for those smaller than 80 μm). The soil's grading curve is presented in Figure 3. Table 5 summarizes the results of the particle size analysis of the studied soil.

Table 5. Morphological characteristics of the soil.

	Grain size distribution proportions (USDA[a])			Curve parameters	
	% Sand	**% Silt**	**% Clay**	C_u	C_c
$d\,[mm]$	$0.05 \le d < 2$	$0.002 \le d < 0.05$	$d < 0.002$	$\frac{D_{60}}{D_{10}}$	$\frac{D_{30}^2}{D_{10} \times D_{60}}$
Value	64.89	15.61	19.5	360	16.47

a. United States Department of Agriculture.

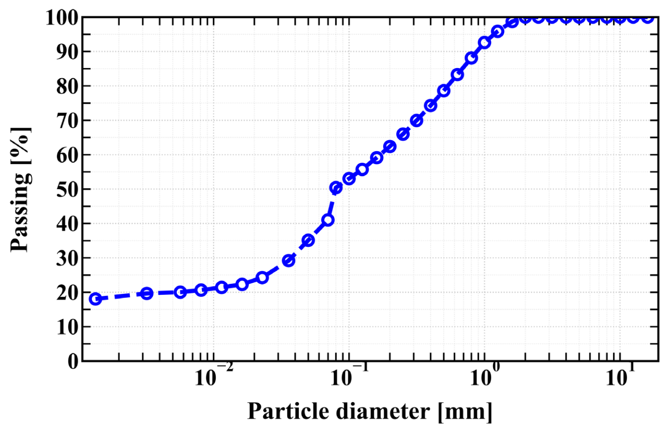

Figure 3. Granulometric curve of soil.

The grain size classification of the soil was performed in accordance with the USDA classification system. The coefficient of uniformity C_u provides an indication of grain size homogeneity: $C_u > 2$ corresponds to a well-graded (extended) distribution, while $C_u < 2$ indicates a uniform distribution. The grading is considered well-graded if $1 < C_c < 3$, and poorly graded otherwise. Based on the values in **Table 5**, the studied material has an extended but poorly graded particle size distribution. The proportion of material passing through the 63 μm sieve is essential for classification according to GTR [27]. This proportion is 39.50%. Being higher than the 35% threshold established by GTR [27], this indicates that the material's behavior is governed by its fine fraction (*i.e.*, particles smaller than 63 μm).

4. Characterization of Thermo-Hydrodynamic Properties

4.1. Thermal Properties—Measurement of Thermal Conductivity

Thermal conductivity is used to describe the thermal behavior of the soil. This parameter is essential for modeling heat transfer within the soil to optimize the design and durability of structures subjected to thermal stresses. The thermal conductivities of the soil in dry (λ_{dry}) and saturated (λ_{sat}) states were measured in the laboratory following standard ASTM-D5334-22 (2022). The specimens used were compacted at optimal conditions: $w = w_{OMC} = 9.4\%$ and $\rho_d = \rho_{dOMC} = 1.98\ g \cdot cm^{-3}$. The dry specimen was prepared in a Proctor mold (Height H = 116.5 mm and Diameter D = 101.5 mm) and subsequently demolded. To ensure uniform and complete drying, it was exposed to ambient air at an average daily temperature of approximately 35˚C for 30 days. It was carefully drilled using a power drill to accommodate the sensor. As for the saturated specimen, it was prepared in an oedometer ring (Height H = 20 mm and Diameter D = 70 mm) and then submerged for 96 hours to achieve full saturation. The KD2 Pro measurement system equipped with the RK-1 sensor, along with the dry and saturated specimens, are shown in **Figure A3** of Appendix A. The RK-1 sensor, with a diameter of 3.9 mm and a length of 6 cm, measures thermal conductivities ranging from 0.10 $W \cdot m^{-1} \cdot K^{-1}$ to 6.00 $W \cdot m^{-1} \cdot K^{-1}$ with an accuracy of ±10%. In accordance with the user manual[1], the sensor was inserted into a hole carefully drilled in each specimen. A reading time of 15 min was set for each of the three (03) measurements performed. The measurement results and the average values are summarized in **Table 6**.

Table 6. Thermal conductivity ($W \cdot m^{-1} \cdot K^{-1}$) of the soil in dry and saturated states.

	Test 1	Test 2	Test 3	Average value
λ_{dry}	0.456	0.461	0.457	0.458
λ_{sat}	1.873	1.814	1.790	1.826

The results show a ratio of approximately 4 (*i.e.*, 1.826/0.458). This discrepancy between λ_{dry} and λ_{sat} is due to the replacement of air (an insulator, $\lambda_{air} \approx 0.024$ $W \cdot m^{-1} \cdot K^{-1}$) with water (a conductor, $\lambda_{water} \approx 0.6$ $W \cdot m^{-1} \cdot K^{-1}$) within the pores during saturation, thereby creating "thermal bridges" between the solid grains.

[1]https://aratajhiz.co/wp-content/uploads/2019/03/13351_KD2-Pro_Web.pdf

Furthermore, the saturated value of 1.826 for λ_{sat} is consistent with soils having a dominant sandy fraction [28].

4.2. Saturated Permeability

The intrinsic permeability k of a soil depends on its geometry as well as the distribution and size of its constituent pores. It is related to the saturated hydraulic conductivity K_{sat} by Equation (1).

$$K_{sat} = k \cdot \frac{\rho \times g}{\mu} \tag{1}$$

where:

- $K_{sat}\left[\mathrm{m \cdot s^{-1}}\right]$ is the saturated hydraulic conductivity of the soil;
- $k\left[\mathrm{m^2}\right]$ is the intrinsic permeability of the soil;
- $\rho\left[\mathrm{kg \cdot m^{-3}}\right]$ is the fluid density;
- $g = 9.81\ \mathrm{m \cdot s^{-2}}$ is the acceleration due to gravity;
- $\mu\left[\mathrm{kg \cdot m^{-1} \cdot s^{-1}}\right]$ is the dynamic viscosity of the fluid.

Direct measurement of intrinsic permeability is complex [29]. Therefore, saturated hydraulic conductivity K_{sat}, which is directly linked to k (Equation (1)), is generally used instead. Experimental laboratory or *in-situ* measurement methods are proposed in the literature for estimating K_{sat}. In this study, K_{sat} is determined using a falling-head permeameter and through a consolidated undrained (CU) triaxial test.

4.2.1. Falling-Head Permeameter Method

Standard NF-X30-441 (2008) specifies the laboratory experimental procedure. The hydraulic conductivity is obtained using Equation (2):

$$K_{sat} = \frac{s}{S}\frac{L}{\Delta t}\ln\left(\frac{h_0}{h_1}\right) \tag{2}$$

where:

- $\Delta t[\mathrm{s}]$ is the time taken by the water to cover the distance $h_0 - h_1[\mathrm{m}]$ (h_0 and h_1 being the initial and final hydraulic heads, respectively);
- s and S are the cross-sectional areas of the standpipe and the specimen, respectively [in $\mathrm{m^2}$];
- $L[\mathrm{m}]$ is the height of the specimen.

4.2.2. Triaxial Test

The triaxial procedure [30] utilizes Darcy's law (Equation (3)), which expresses the volumetric flow rate Q [$\mathrm{m^3 \cdot s^{-1}}$] (or the filtration velocity of water through the soil column) as a function of the cross-sectional area A [$\mathrm{m^2}$] of the specimen and the hydraulic gradient $i = \Delta h / L$:

$$Q = K_{sat} \cdot A \cdot i \tag{3}$$

where Δh [m] is the head loss. **Figure 4** shows the evolution of the volume of water injected into the soil specimen during the test at a pressure of 79 kPa. The volumetric flow rate Q corresponds to the slope of the resulting linear trend line. The measurement characteristics for K_{sat} are presented in Table 7.

Table 7. Permeability measurement characteristics.

$Q\left[m^3 \cdot s^{-1}\right]$	$A\left[m^2\right]$	$\Delta h[m]$	$L[m]$	$i[/]$
$6.00 \cdot 10^{-9}$	$3.85 \cdot 10^{-3}$	7.76	0.14	55.43

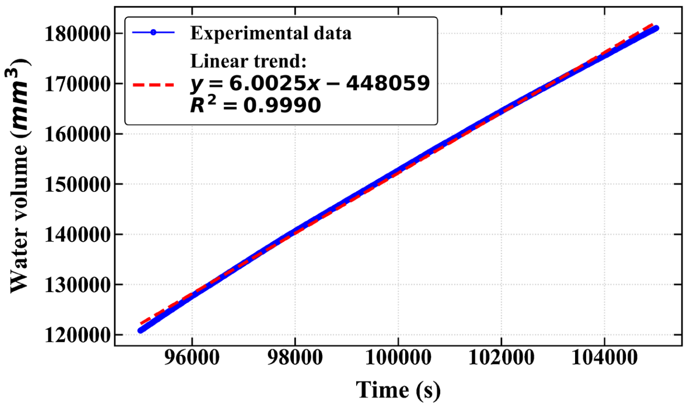

Figure 4. Variation of water volume as a function of time.

4.2.3. Results

The measurement results for the soil's hydraulic conductivity are presented in Table 8. The obtained experimental values of K_{sat} are relatively close, with a mean relative difference of 2.09%. These values, on the order of 10^{-8} m·s^{-1}, are typical of a clayey to silty clay soil.

Table 8. Hydraulic conductivity and intrinsic permeability of the soil.

Test	$K_{sat}\left[m \cdot s^{-1}\right]$	$k\left[m^2\right] = \frac{\mu}{\rho g} \cdot K_{sat}$
Permeameter	$2.93 \cdot 10^{-8}$	$2.99 \cdot 10^{-15}$
Triaxial test	$2.81 \cdot 10^{-8}$	$2.86 \cdot 10^{-15}$

4.3. Soil-Water Characteristic Curve

The ability of a soil to retain or release its pore water is characterized by the determination of the soil-water characteristic curve (SWCC). It is typically represented in an (S_r, s) or (w, s) plane for a given void ratio e_0. The experimental setup for measuring suction at a given water content differs for low and high suction ranges. A synthesis of the challenges regarding the experimental and numerical (modeling) determination of the characteristic curve is presented in [29], with an emphasis on determination across the entire water content range: from the saturated state to the near-dry state. The WP4C chilled-mirror dewpoint potentiometer (Figure A4 of Appendix A) was used in our study. Unlike other methods such as the pressure plate apparatus (Richards pressure chamber), this device measures total soil suction over a range from 100 kPa to $3 \cdot 10^5$ kPa. The experimental procedure complies with the standard ASTM-D6836-16 (2016). Its operating principle is based on measuring the relative humidity of air at the dew point inside a sealed chamber containing the soil specimen at equilibrium García Fernández *et al.* [31]. Kelvin's law (Equation (4)) is then applied to estimate the total soil suction Ψ (the sum of a matric component Ψ_m due to the porous matrix and capillary forces, and an osmotic component Ψ_O due to solute concentration in the pore fluid). In this study, osmotic effects were neglected because at low water contents, the measured suction is dominated by capillary and matric effects; furthermore, demineralized water was used in specimen preparation, thereby limiting the presence of soluble salts [32] [33]. Consequently, the suction measured by the WP4C is assumed to be the matric suction ($\Psi_m \approx \Psi = -s$).

$$s = -\frac{RT\rho_w}{M_w}\ln\left(RH\right) \tag{4}$$

where:

- $s\left[\text{MPa}\right]$ is the matric suction;
- $R = 8.3143\ \text{J}\cdot\text{K}^{-1}\cdot\text{mol}^{-1}$ is the ideal gas constant;
- $T\left[\text{K}\right]$ is the absolute temperature;
- $M_w = 0.01801\ \text{kg}\cdot\text{mol}^{-1}$ is the molar mass of water;
- $\rho_w = 998\ \text{kg}\cdot\text{m}^{-3}$ is the density of pure water at 293 K; and;
- $RH\,[/]$ is the relative humidity.

Figure 5 presents the experimental retention curves alongside those estimated by the numerical model (Equation (5)) of Van Genuchten [34] (the most widely used in the literature). Discrepancies between the experimental and simulated curves are observed for water contents exceeding 50%. These gaps are explained by the inaccuracy of suction measurements in this range, as the WP4C is particularly suited for high suctions. The model calibration parameters (Equation (5)) and the associated statistical test results (R^2 and Root Mean Square Error: RMSE) are presented in **Table 9**.

$$S_e = \frac{S_l - S_{\min}}{S_{\max} - S_{\min}} = \left[1 + \left(\frac{s}{P}\right)^{\frac{1}{1-\lambda}}\right]^{-\lambda} \tag{5}$$

where:

- $S_e\left[/\right]$ is the effective degree of saturation of the soil;
- $S_l\left[/\right]$ is the liquid (water) saturation;
- $S_{\max}\left[/\right]$ is the maximum saturation;
- $S_{\min}\left[/\right]$ is the minimum (or residual) saturation;
- $s\left[\text{MPa}\right]$ is the matric suction;
- $P\left[\text{MPa}\right]$ and $\lambda\left[/\right]$ are constant parameters to be determined from the experimental curve.

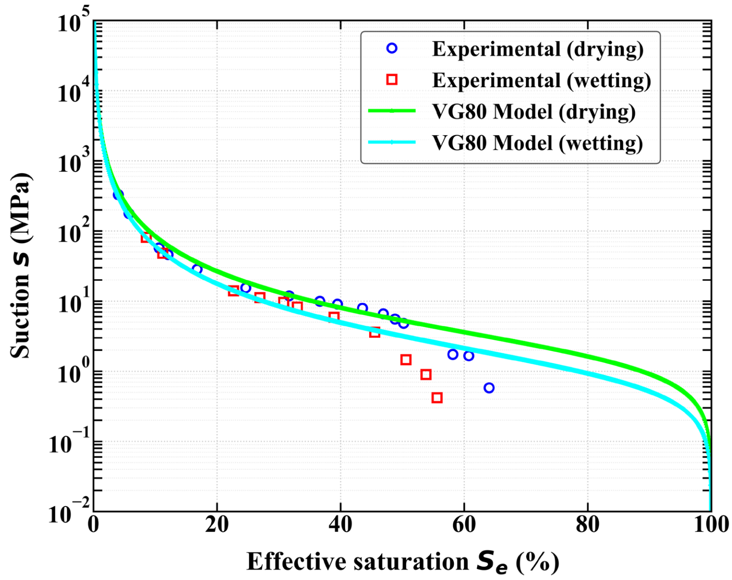

Figure 5. Soil-water characteristic curve.

Table 9. Van Genuchten model parameters [34] for the characteristic curve.

	P	λ	R^2	RMSE
Drying	1.85	0.375	0.9993	2.4
Wetting	1.03	0.361	0.9978	1.3

The discrepancy between $P_{\text{dry}} = 1.85\ \text{MPa}$ and $P_{\text{wet}} = 1.03\ \text{MPa}$ indicates that the soil releases its water more with more difficulty than it reabsorbs it. This behavior is conventionally attributed to changes in the contact angle during the drying-wetting cycle. The higher value of P_{dry} suggests a degree of hydraulic inertia during desiccation episodes.

From a practical standpoint, this property could be a potentially favorable factor for embankment stability under alternating dry and wet seasons. Indeed, since desaturating the material is more difficult ($P_{\text{dry}} > P_{\text{wet}}$), the suction variations induced by climatic cycles could be limited—and consequently, variations in effective stress—thereby reducing the risk of shrink-swell behavior. However, it should be emphasized that *in situ* stability cannot be captured by the retention curve alone, as it depends on several other parameters (geometry, drainage conditions, cohesion, friction angle, and dynamic loading). The work of Kocaman *et al.* [35] and Luo *et al.* [36] indicates that pores associated with higher values of P or suction (several hundred kPa) fall within the range of micropores and ultramicropores, which are typical of fine-grained structures. A parameter P of 1.85 MPa thus indicates fine pores, confirming the presence of the clay fraction identified earlier.

5. Soil Bearing Indices

The bearing capacity of a soil is a measure of its ability to support mechanical loads applied to its surface. It is evaluated using the California Bearing Ratio (CBR) and the Immediate Bearing Index (IBI). These bearing indices are used to establish soil utilization criteria in road engineering, as well as to evaluate the trafficability of earthmoving equipment and the thickness of pavement layers based on the underlying soil, expected traffic, anticipated loads, and future hydraulic conditions [22]. In the present study, the soaked CBR and IBI indices were determined for compaction energies corresponding to 25 blows/layer and 56 blows/layer. The tests were conducted on a single soil sample. The characteristics of the IPI and soaked CBR specimens, as well as the test results, are recorded in **Table 10**.

Table 10. Results of soaked CBR and IBI tests.

Test	Parameters	25 blows	56 blows
IPI	$w_{\text{initial}}[\%]$	7.8	8.3
	$I_{\text{IBI}}[\%]$	25	50
	$\rho_d\left[\text{g}\cdot\text{cm}^{-3}\right]$	2.04	2.07
	Degree of compaction [%]	97.14	98.57
Soaked CBR	$w_{\text{initial}}[\%]$	7.8	7.9
	$I_{\text{CBR}}[\%]$	17	20
	$\rho_d\left[\text{g}\cdot\text{cm}^{-3}\right]$	2.00	2.09
	Degree of compaction [%]	95.24	99.52
	$G=\Delta H/H[\%]$	0.12	0.03
	$w_{\text{final}}[\%]$	10.18	12.30

The values of the bearing indices I_{CBR} and I_{IBI} indicate a soil of medium bearing capacity. According to the I_{CBR} index, the studied soil belongs to bearing class S4 [37]. The same class was obtained by Mbengue *et al.* [21] for a borrow pit in Saaba (located on the map in **Figure 1**). The linear swell index G, being less than 1%, falls within the allowable range for pavement layers [37]. The soil bearing capacity drops significantly after soaking, decreasing from $I_{\text{IBI}}=50\%$ to $I_{\text{CBR}}=20\%$ (a 30% reduction) for 56-blow compaction, and from $I_{\text{IBI}}=25\%$ to $I_{\text{CBR}}=17\%$ (an 8% reduction) for 25-blow compaction. This drop indicates that at saturation (immersion), the matric suction vanishes. The apparent cohesion provided by suction disappears, leaving the soil to rely solely on its internal friction (sandy fraction) and its intrinsic cohesion (clay fraction). However, this reduction is low compared to bearing capacity losses of 77% and 82% reported by Bâ *et al.* [38] for lateritic soil samples in Senegal. This difference may be explained by the low activity of the clay fraction in the soil under study. This activity is assessed by Skempton's activity index (A_c), which evaluates the soil's reactivity to changes in hydraulic states: $A_C=I_P/C_{2\mu\text{m}}=0.95$. This result corresponds to a moderately active clay [39]. **Figure 6** shows the evolution of the I_{CBR} and I_{IBI} bearing indices according to the compaction level. The evolution of the IBI index in **Figure 6(a)** demonstrates that the soil requires intense compaction (Modified Proctor energy) to achieve its maximum density. According to the evolution of the I_{CBR} index (**Figure 6(b)**), such compaction could enable the soil to maintain its bearing capacity in the event of significant changes in hydraulic conditions. Nevertheless, the risk of swelling or a decrease in bearing capacity should not be entirely ruled out.

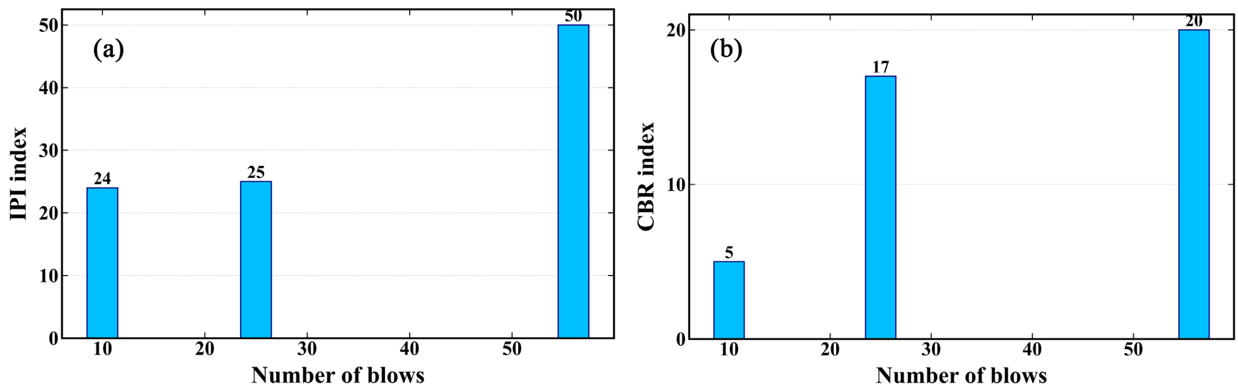

Figure 6. Variations in bearing indices as a function of compaction energy: (a) IBI index and (b) CBR index.

6. Classification of the Studied Material

The soil characterization tests presented in the preceding sections provided the parameters necessary for its classification. Thus, the soil classes according to the [27], LCPC (Laboratoire Central des Ponts et Chaussées), and lateritic classification [23] are presented in **Tables 11-13**, respectively.

Table 11. GTR soil class [27].

Identification	Grading justifications	Classification
Soil with: $D_{max} = 20$ mm passing 63 µm: 35.5%; $I_P = 15.6\%$; $C_u = 545.45 > 6$	Sandy fraction 0.063/2 mm (51.1%) > gravelly fraction 2/63 mm (13.4%)	**F2** **clay or silty fine sand with extended grading**

Table 12. LCPC soil class.

Grading justifications	Conditions	Geotechnical designation
$d \geq 2$ mm $= 13.4\%$; 80 µm $< d <$ 2 mm $= 42.8\%$; $d \leq 80$ µm $= 43.8\%$	$w_L = 31.7\%$ and $I_P = 15.6\%$	**SA** **sandy clay**

Table 13. Lateritic soil class [23].

Grading justification	Conditions	Lateritic class
Passing 80 µm: 43.8% > 30%	MBV = 1.5 and $w_P = 16.1\%$ then $w_R = SL < 20\%$; $I_{CBR} = 20\%$	**SLF$_{L1}$** **fine silty lateritic soil**

Based on the classification criteria used by the different systems, the soil in this study is identified as a clayey sandy silt. This classification is consistent with the particle size proportions (**Table 5**). The USDA triangular diagram places it within the aforementioned class. The behavior of this material, while dominated by the sandy fraction, shows a significant influence from the clay content. According to the [27] guide, this soil is suitable for use in road earthworks. However, its implementation is subject to either prior treatment or strict compliance with the recommendations of "Fascicule 2" [27].

7. Conclusions

This study contributes to the valorization of road cut materials in Sub-Saharan Africa through a detailed characterization of an excavated soil from a road construction site in Ouagadougou (Burkina Faso). The work carried out enabled an integrated assessment of the physical, morphological, thermal, and hydrodynamic properties of the soil. Through this characterization, the parameters necessary for classifying the material within established systems were identified. The systems selected for soil identification were: the Guide for Earthworks (GTR), the classification system of the Laboratoire Central des Ponts et Chaussées (LCPC), and the classification system for lateritic materials in tropical regions proposed by Reiffsteck *et al.* [23]. The material was classified as follows:

- According to the GTR: a fine, moderately sandy clay with extended grading;
- According to the LCPC classification: a low-plasticity sandy clay;
- According to the lateritic soil classification by Reiffsteck *et al.* [23]: a fine silty lateritic soil (SLF_{L1}).

Despite being traditionally classified as "mediocre", the F2 material provides sufficient immediate bearing capacity for earthwork applications. Its reuse helps limit the opening of new lateritic borrow pits, significantly reducing the project's ecological footprint. However, achieving efficient implementation requires prior treatment or strict adherence to the GTR guidelines [27].

Acknowledgements

This work is part of Burkina Faso's Higher Education Support Project (PAES), funded by the World Bank, and is the result of a collaboration between Joseph KI-ZERBO University, the 2iE institute, and the Polytechnic University of Catalonia (UPC).

Author Contributions

Conceptualization, Soumaïla Gandema and François Dabilgou; methodology, Soumaïla Gandema and Marcel Bawindsom Kébré; validation, Marcel Bawindsom Kébré; formal analysis, Marcel Bawindsom Kébré and Adamah Messan; investigation, Soumaïla Gandema; resources, Soumaïla Gandema and Marcel Bawindsom Kébré; data curation, Soumaïla Gandema; writing—original draft preparation, Soumaïla Gandema; writing—review and editing, Soumaïla Gandema, Marcel Bawindsom Kébré, Guillaume Zamantakonè Ki and Marie Therese Marame Mbengue; visualization, Soumaïla Gandema; supervision, Marcel Bawindsom Kébré and Marie Therese Marame Mbengue; project administration, Marcel Bawindsom Kébré, Marie Therese Marame Mbengue, Rimyalegdo Kiébré and Adamah Messan; funding acquisition, Marcel Bawindsom Kébré and Adamah Messan. All authors have read and agreed to the published version of the manuscript.

Conflicts of Interest

The authors declare no conflicts of interest regarding the publication of this paper.

References

[1] Rapport-MI (2024) Bulletin statistique trimestriel des infrastructures de transport (Ministère des infrastructures, Burkina Faso). Rapport.

[2] AGETIB (2024) Projet multinational Burkina—Côte d'Ivoire Mali, Programme d'interconnexion des routes communautaires et de facilitation des transport/travaux de renforcement de la section de la route communautaire CU7B Bobo-Dioulasso—Banfora—Frontière du Mali (155km) y compris l'amenagement et le bitumage de la bretelle Banfora—Orodara (42km) et travaux connexes: Notice d'impact environnemental et social (NIES) des travaux d'amenagement de 50km de pistes rurales dans les regions des Cascades et des Hauts bassins (Rapport définitif). https://www.infrastructures.gov.bf/document

[3] PNDES-II (2021) Plan national de développement économique et social 2021-2025 (Burkina Faso). Rapport.

[4] Foko Tamba, C., Kengni, L. and Tematio, P. (2023) Geotechnical Suitability of Soils in Road Construction for Sustainable Development in Tropical Africa: Case of Lateritic Graveled Soils of Bandjoun (West, Cameroon). *Advances in Civil Engineering*, **2023**, 1-14. https://doi.org/10.1155/2023/6662521

[5] Fongang, B.T., Tassongwa, B., Manefouet, B.I., Yemeli, C.M. and Ngapgue, F. (2022) Contribution to the Flexible Pavement Design Guides Evaluation Used in Tropical Zone: Application to Lateritic Materials of Bamougoum (West, Cameroon). *Case Studies in Construction Materials*, **16**, e01064. https://doi.org/10.1016/j.cscm.2022.e01064

[6] Corté, J.F., Baraize, E., Gautier, J.L., Lebouteiller, E., Maïga, O., Kouassi, P., Tessilimi, M. and Toe, J.M. (2019) Revue du Guide pratique de dimensionnement des chaussées pour les pays tropicaux—Rapport technique (AIPCR). https://www.piarc.org/fr/activites/Catalogue-Rapports-Techniques-PIARC

[7] Bazame, R., Tanrıvermis, H. and Kapusuz, Y.E. (2019) Land Management and Sustainable Use of Land Resources in the Case of Burkina Faso. *Land Degradation & Development*, **30**, 608-621. https://doi.org/10.1002/ldr.3247

[8] Naba, C., Ishidaira, H., Magome, J. and Souma, K. (2024) Exploring the Potential of Soil and Water Conservation Measures for Climate Resilience in Burkina Faso. *Sustainability*, **16**, Article 7995. https://doi.org/10.3390/su16187995

[9] Daku, S.S., Igwe, O. and Bala, D.A. (2024) Geotechnical, Geochemical and Mineralogical Evaluations of Mine Spoils of the Jos-Bukuru Tin Field, Central Nigeria: Implications for Utilization as Road Construction Material. *Scientia Africana*, **23**, 33-50. https://doi.org/10.4314/sa.v23i4.3

[10] Gansonré, Y., Breul, P., Bacconnet, C., Benz, M. and Gourvès, R. (2021) Estimation of Lateritic Soils Elastic Modulus from CBR Index for Pavement Engineering in Burkina Faso. *International Journal of Pavement Research and Technology*, **14**, 348-356. https://doi.org/10.1007/s42947-020-0118-9

[11] Ogochukwu Okeke, E., Pius Aghamelu, O., Victor Omonona, O. and Christine Ozougwu, C. (2025) Quality of Construction Materials and Their Effects on the Sustainability of Highway Pavements in Parts of Anambra State, Southeastern Nigeria. *Global Journal of Geological Sciences*, **23**, 31-48. https://doi.org/10.4314/gjgs.v23i1.3

[12] Penka, J.B., Nana, U.J.M.P., Manjia, M.B., Bomeni, I.Y. and Pettang, C. (2022) Hydrological, Mineralogical and Geotechnical Characterisation of Soils from Douala (Coastal, Cameroon): Potential Used in Road Construction. *Heliyon*, **8**, e11287. https://doi.org/10.1016/j.heliyon.2022.e11287

[13] Azizi, A., Kumar, A. and Toll, D.G. (2021) Coupling Cyclic and Water Retention Response of a Clayey Sand Subjected to Traffic and Environmental Cycles. *Géotechnique*, **73**, 401-417. https://doi.org/10.1680/jgeot.21.00063

[14] Li, D., Wang, Z., Jia, Z., Bu, W., Sun, Q. and Wang, Z. (2024) Experimental Study on Deformation Characteristics of Seasonal Subgrade Soil under Dynamic Load. *PLOS ONE*, **19**, e0309443. https://doi.org/10.1371/journal.pone.0309443

[15] Ng, C.W.W., Wang, Y., Zhang, S. and Zhang, Q. (2024) Effects of Climate Change on Soil Embankments for Transport Infrastructure. *Transportation Geotechnics*, **48**, Article 101324. https://doi.org/10.1016/j.trgeo.2024.101324

[16] Mengue, E., Mroueh, H., Lancelot, L. and Eko, R.M. (2017) Mechanical Improvement of a Fine-Grained Lateritic Soil Treated with Cement for Use in Road Construction. *Journal of Materials in Civil Engineering*, **29**, Article 04017206. https://doi.org/10.1061/(asce)mt.1943-5533.0002059

[17] Mengue, E., Mroueh, H., Lancelot, L. and Eko, R.M. (2018) Design and Parametric Study of a Pavement Foundation Layer Made of Cement-Treated Fine-Grained Lateritic Soil. *Soils and Foundations*, **58**, 666-677. https://doi.org/10.1016/j.sandf.2018.02.025

[18] Abdeldjalil, M., Bensekhria, A. and Akacem, M. (2024) Identification of Dune Sands Used in Building by Their Characteristics and a Granular Model for an Arid Environment. *Asian Journal of Civil Engineering*, **25**, 2883-2901. https://doi.org/10.1007/s42107-023-00951-4

[19] Daheur, E.G., Taibi, S., Goual, I. and Li, Z.S. (2021) Hydro-Mechanical Behavior from Small Strain to Failure of Tuffs Amended with Dune Sand—Application to Pavements Design in Saharan Areas. *Construction and Building Materials*, **272**, Article 121948. https://doi.org/10.1016/j.conbuildmat.2020.121948

[20] Daheur, E.G., Li, Z.S., Demdoum, A., Taibi, S. and Goual, I. (2023) Valorisation of Dune Sand-Tuff for Saharan Pavement Design. *Construction and Building Materials*, **366**, Article 130239. https://doi.org/10.1016/j.conbuildmat.2022.130239

[21] Mbengue, M.T.M., Gana, A.L., Messan, A. and Pantet, A. (2022) Geotechnical and Mechanical Characterization of Lateritic Soil Improved with Crushed Granite. *Civil Engineering Journal*, **8**, 843-862. https://doi.org/10.28991/cej-2022-08-05-01

[22] Mbengue, M.T.M., Gana, A.L., Messan, A., Mone, O. and Pantet, A. (2023) Effect of the Type of Lateritic Soil on the Effectiveness of Geomechanical Improvement Using a Low Quantity of Cement for Sustainable Road Construction. *Materials*, **16**, Article 6891. https://doi.org/10.3390/ma16216891

[23] Reiffsteck, P., Auriol, J.C., Ndiaye, M. and Rodrigues, J.K.G. (2010) Rationalisation

de l'Utilisation des Sols Latéritiques en Plateforme de Chaussées Durables et de Faible Coût. 28*èmes Rencontres Universitaires de Génie Civil*, La Bourboule, 2-4 June 2010. https://hal.science/hal-00508850

[24] Savadogo, N., Traoré, Y.B., Karoré, W.I., Gana, L.A. and Nshimiyimana, P. (2024) Investigation of the Effects of Fine Dune Sand on the Geotechnical Characteristics of Lateritic Soil. *World Journal of Advanced Research and Reviews*, **23**, 1065-1074. https://doi.org/10.30574/wjarr.2024.23.1.1948

[25] Savadogo, N., Traoré, Y.B., Kocty, R. and Moné, O. (2024) Stabilization of Lateritic Soil with Portland Cement and Crushed Granite for Pavement Base Courses. *World Journal of Advanced Research and Reviews*, **23**, 3090-3099. https://doi.org/10.30574/wjarr.2024.23.3.2914

[26] Bellagh, K., Lenoir, T., Paulus, H., Duc, M., L'Huillier, E., Gotteland, P. and Magnan, J.P. (2016) Caractérisation de sols urbains pour une utilisation en terrassement routier. https://hal.science/hal-02882278

[27] GTR (2023) Guide des terrassements des remblais et des couches de forme: Fascicule No. 1—Principes généraux/Fascicule No. 2—Annexes techniques Édition 2024.

[28] Li, L., Lu, Y., Ren, T. and Horton, R. (2023) Quartz Contents Derived from Particle Density Measurements Improve the Accuracy of Soil Thermal Conductivity Estimates. *Geoderma*, **436**, Article 116526. https://doi.org/10.1016/j.geoderma.2023.116526

[29] Kébré, M.B., Ouedraogo, F., Betaboalé, N., Zougmoré, F. and Cherblanc, F. (2013) Soil-Water Characteristic Curve Modeling at Low Water Content: Empirical and Semi-Empirical Approaches. *International Journal of Engineering Research*, **2**, 432-437.

[30] Rees, S. (2013) Part One: Introduction to Triaxial Testing. GDS Website.

[31] Garcia-Fernandez, C.C., Cardoso, R., Alvarez-Fernandez, M.I. and Gonzalez-Nicieza, C. (2020) Changes on Diametral Compression Behaviour of Compacted Marls Due to Drying. *E3S Web of Conferences*, **195**, Article 03008. https://doi.org/10.1051/e3sconf/202019503008

[32] Ying, Z., Benahmed, N., Cui, Y.J. and Duc, M. (2022) Determining Osmotic Suction through Electrical Conductivity for Unsaturated Low-Plasticity Soils. *Journal of Rock Mechanics and Geotechnical Engineering*, **14**, 1946-1955. https://doi.org/10.1016/j.jrmge.2021.12.020

[33] Lu, Y., Abuel-Naga, H., Leong, E. and Shang, Z.C. (2023) Reliability of Chilled-Mirror Hygrometer (WP4C) for Soil Total Suction Measurement. *Geotechnical Testing Journal*, **47**, 733-752. https://doi.org/10.1520/gtj20230387

[34] van Genuchten, M.T. (1980) A Closed-Form Equation for Predicting the Hydraulic Conductivity of Unsaturated Soils. *Soil Science Society of America Journal*, **44**, 892-898. https://doi.org/10.2136/sssaj1980.03615995004400050002x

[35] Kocaman, K., Ozocak, A., Edil, T.B., Bol, E., Sert, S., Onturk, K., *et al.* (2022) Evaluation of Soil-Water Characteristic Curve and Pore-Size Distribution of Fine-Grained Soils. *Water*, **14**, Article 3445. https://doi.org/10.3390/w14213445

[36] Luo, S., Zhou, B., Likos, W.J. and Lu, N. (2024) Determining Capillary Pore–size Distribution of Soil from Soil-Water Retention Curve. *Journal of Geotechnical and Geoenvironmental Engineering*, **150**, Article 0402318. https://doi.org/10.1061/jggefk.gteng-11647

[37] CEBTP (1984) Guide pratique de dimensionnement des chaussées pour les pays tropicaux. CEBTP (Centre Expérimental du Bâtiment et de Travaux Publics): Paris,

France.

[38] Bâ, M., Ki, B.I.J. and Sall, O.A. (2023) Resilient Modulus of Compacted Granular and Lateritic Materials Used as Base Layers for Flexible Pavements in West Africa. *International Journal of Research and Review*, **10**, 254-259. https://doi.org/10.52403/ijrr.20231130

[39] Ratrimoarisonina, H.A., Ramaleoharinjato, J., Randriamalala, T.R. and Rakotovololona, F. (2019) Contribution a la mise en place d'un systeme de gestion de base de donnees de lateritede la region analamanga madagascar. https://hal.science/hal-02278369

Appendix A. Illustrations of Select Experimental Equipment and Procedures

Figure A1. One of four (4) disposal sites for materials excavated from the road construction site.

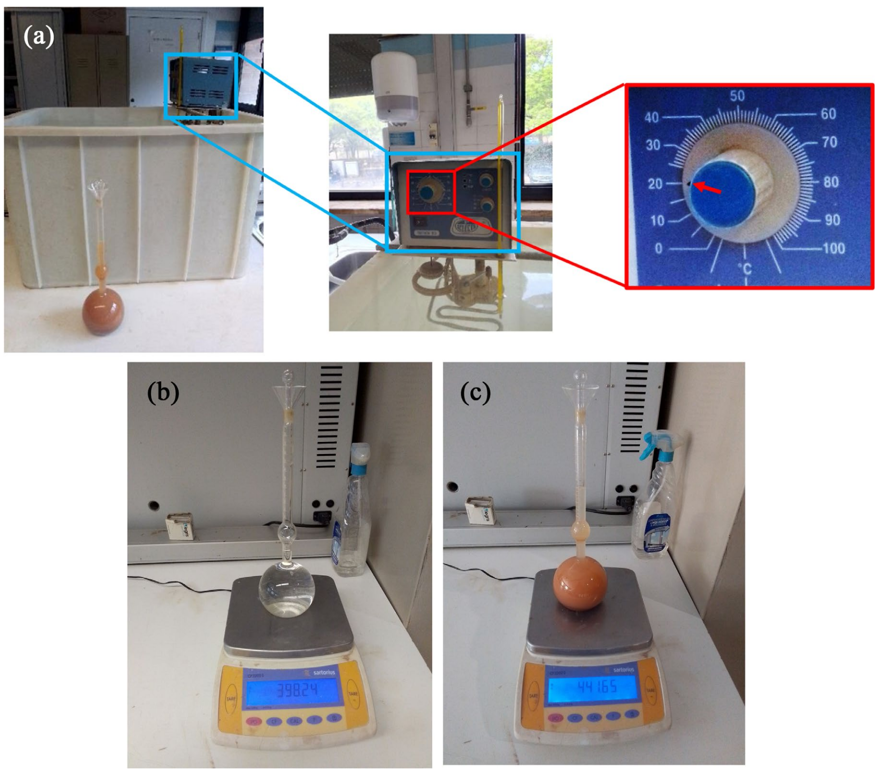

Figure A2. Water pycnometer for determining particle density: (a) water bath and temperature control unit set to maintain a constant temperature (20 ˚C in this test), (b) mass and volume of liquid (pure ethanol), and (c) mass and volume of liquid plus material.

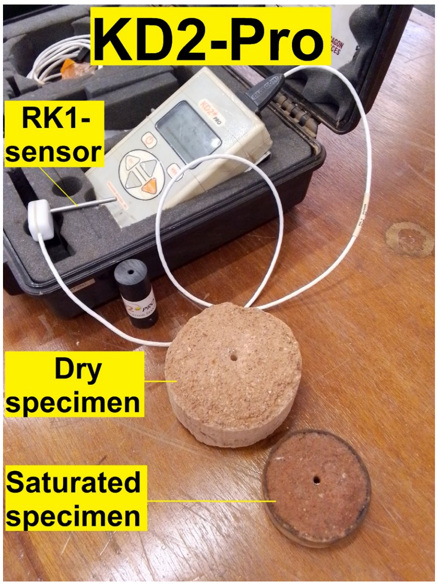

Figure A3. Thermal conductivity measurement in dry and saturated states: KD2 Pro testing system with dry and saturated specimens.

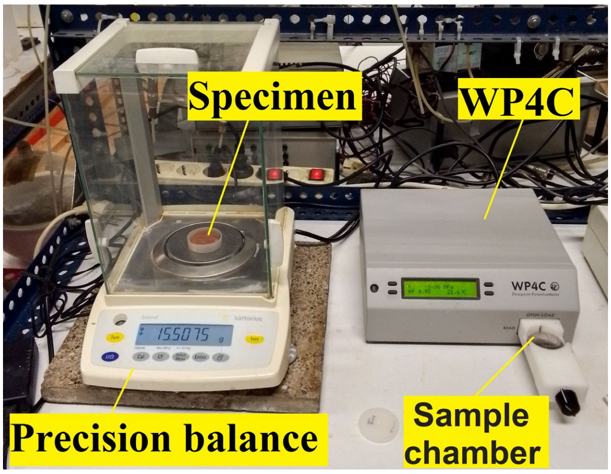

Figure A4. Experimental setup for the characteristic curve (WP4C & precision electronic balance containing the soil sample).